Documentation of open-source MFIX–PIC software for gas-solids flows [1]

R. Garg
Rahul.Garg@netl.doe.gov
National Energy Technology Laboratory, Morgantown, WV 26505, U.S.A.
URS Energy & Construction, Morgantown, WV 26505, U.S.A.

J. F. Dietiker
Jeff.Dietiker@netl.doe.gov
National Energy Technology Laboratory Morgantown, WV 26505, U.S.A.
West Virginia University Research Corporation, Morgantown, WV 26506, U.S.A.

February 22, 2013

[1]Refer to this document as: R. Garg, J. F. Dietiker, Documentation of open-source MFIX–PIC software for gas-solids flows, From URL `https://mfix.netl.doe.gov/documentation/mfix_pic_doc.pdf`

Table of Contents

1 Introduction and Background

This is a short documentation of the MPPIC model recently implemented in MFIX. The model is still under development and activities are on going to validate the model. In the next few sections, the governing equations solved in MPPIC model are discussed. Of particular interest in MPPIC model is the implementation of frictional stress model. In section 3, the implementation of frictional stress model in past studies is discussed which is followed (Section 4) by the discussion of the newly implemented frictional stress model in the MFIX's MPPIC model implementation. The computational details of the MPPIC model implementation are given in section 5. In section 6, some preliminary results from a bubbling bed case are discussed. This is a living document and will be updated based on new improvements made in-house at NETL or from MFIX's user community. In the nomenclature adopted for this documentation, MFIX refers to Eulerian-Eulerian model, MFIX-DEM refers to Eulerian model for carrier phase and soft-spring based discrete element model (DEM) for the dispersed phase, and MFIX-PIC refers to Eulerian model for carrier phase coupled with particle-in-cell (PIC) based discrete representation for dispersed phase.

2 Governing Equations

In MFIX-PIC, the gas-phase governing equations for mass and momentum conservation are similar to those in traditional gas-phase CFD but with additional coupling terms due to drag from the solids-phase. The solids-phase is modeled using discrete particles. Below we provide the list of governing equations along with the numerical implementation including the coupling procedure.

2.1 Gas-phase

The governing equations, implemented in MFIX (Syamlal et al., 1993), for the gas-phase continuity and momentum conservation in the absence of phase change, chemical reactions, growth, aggregation, breakage phenomena, are:

$$\frac{\partial(\varepsilon_{\rm g}\rho_{\rm g})}{\partial t} + \boldsymbol{\nabla}\cdot(\varepsilon_{\rm g}\rho_{\rm g}\mathbf{v}_{\rm g}) = 0 \quad ; \tag{1}$$

and

$$\frac{D}{Dt}(\varepsilon_{\rm g}\rho_{\rm g}\mathbf{v}_{\rm g}) = \boldsymbol{\nabla}\cdot\overline{\overline{S}}_{\rm g} + \varepsilon_{\rm g}\rho_{\rm g}\mathbf{g} - \sum_{m=1}^{M}\mathbf{I}_{{\rm g}m} \quad . \tag{2}$$

In the above equation, $\varepsilon_{\rm g}$ is the gas-phase volume fraction, $\rho_{\rm g}$ is the thermodynamic density of the gas phase, $\mathbf{v}_{\rm g}$ is the volume-averaged gas-phase velocity, $\mathbf{I}_{{\rm g}m}$ is the momentum transfer term between the gas and the $m^{\rm th}$ solid phase, and $\overline{\overline{S}}_{\rm g}$ is the gas-phase stress tensor given by

$$\overline{\overline{S}}_{\rm g} = -P_{\rm g}\overline{\overline{I}} + \overline{\overline{\tau}}_{\rm g}, \tag{3}$$

where $P_{\rm g}$ is the gas-phase pressure. Also, $\overline{\overline{\tau}}_{\rm g}$ is the gas-phase shear stress tensor,

$$\overline{\overline{\tau}}_{\rm g} = 2\mu_{\rm g}\overline{\overline{D}}_{\rm g} + \lambda_{\rm g}\boldsymbol{\nabla}\cdot{\rm tr}(\overline{\overline{D}}_{\rm g})\overline{\overline{I}}, \tag{4}$$

where $\overline{\overline{D}}_{\rm g} = \frac{1}{2}\left[\boldsymbol{\nabla}\mathbf{v}_{\rm g} + (\boldsymbol{\nabla}\mathbf{v}_{\rm g})^T\right]$ is the strain rate tensor, and μ_g and λ_g are the dynamic and second coefficients of viscosity of the gas phase.

2.2 Solid-phase: MPPIC method

In the MPPIC approach, each solid phase is represented in discrete manner by notional particles/parcels that are mapped to the physical system through the idea of statistical weight. In this approach, the m^{th} solid-phase is represented by N_m parcels with each parcel having diameter D_m and density ρ_{sm} which are equal to the diameter and density of the m^{th} solid-phase. For total of M solid phases, the total number of parcels is equal to $N = \sum_{m=1}^{M} N_m$. These N parcels are represented in a Lagrangian frame of reference at time t by $\{\mathbf{X}_{\text{p}}^{(i)}(t), \mathbf{V}_{\text{p}}^{(i)}(t), D_{\text{p}}^{(i)}, \rho_{\text{p}}^{(i)}, W_{\text{p}}^{(i)}(t),\ i = 1, \ldots, N\}$, where $\mathbf{X}_{\text{p}}^{(i)}(t)$ denotes the i^{th} parcel's position, $\mathbf{V}_{\text{p}}^{(i)}(t)$ denotes its linear velocity, $D_{\text{p}}^{(i)}$ denotes its diameter, $\rho_{\text{p}}^{(i)}$ represents its density, and $W_{\text{p}}^{(i)}$ denotes its statistical weight which is discussed below in more detail. It is implicit that if a parcel belongs to m^{th} solid–phase, then its diameter and density are, respectively, equal to D_m and ρ_{sm} (i.e., equal to the diameter and density of the m^{th} solid–phase).

In the MPPIC model, $W_{\text{p}}^{(i)}$ is the number of real particles represented by a parcel. Value of one for $W_{\text{p}}^{(i)}$ implies one-to-one correspondence between real particles and parcels, i.e., each parcel represents one real particle. Value of less than one implies that a parcel carries less than one real particle. This is possible either by choice in dilute systems (to reduce the statistical errors arising from estimation of mean fields) or due to chemical reactions. Value of greater than one implies that a parcel represents more than one real particle. For dense or device scale applications, where the real number of particles could be computationally intractable, values greater than one for statistical weight reduces the number of discrete entities (and hence the computational cost) whose Lagrangian trajectories have to be tracked. Since the current study is limited to non-reactive flows, the statistical weight of parcels does not evolve.

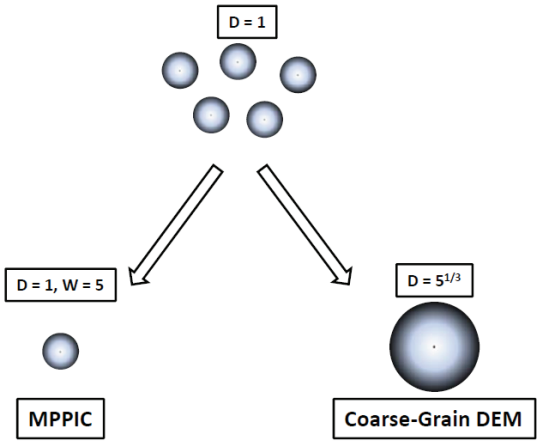

Figure 1: Schematic showing the difference between the MPPIC and coarse-grain DEM approach. In the MPPIC approach (left), 5 spherical particles having diameter of 1 unit are represented by a single parcel having diameter of 1 unit and statistical weight equal to 5. However, in the coarse-grain DEM approach, they are represented by a larger spherical parcel having diameter of $5^{1/3}$ units which is obtained by equating the volume of tracked parcel to the sum of volumes of individual particles.

Although the representation of several real particles by one parcel in MPPIC model significantly reduces the computational cost, the same simplification also results in severe loss of physical phenomena that, if not modeled accurately, are not naturally captured in CFD simulations using MPPIC model. For example, the inter particle collisions for particles making up the parcel are not resolved. Likewise, inter-parcel collisions also need to be modeled. A slightly variant approach to MPPIC model is the coarse-grain DEM model, first put forward by Patankar and Joseph (2001). Similar to MPPIC model, even in this model many real particles are combined to form one parcel and, as shown in Fig. 1, a parcel's diameter is set by equating the volume of parcel to the sum of volumes of real particles that make up the parcel. The parcels are then tracked in a Lagrangian manner and inter-parcel collisions are resolved using the soft-spring model (Cundall and Strack, 1978). The advantage of such an approach is that inter-parcel collisions are directly resolved. As will be discussed later, one of the most critical issues affecting the stability of MPPIC model is a robust solids pressure term that prevents solids packing over the physically allowed maximum values. Since the inter-parcel collisions are directly resolved in coarse-grain DEM model, like in the standard DEM model, there is no need to model solids pressure term to prevent over packing. However, this method still suffers from the ills of soft-spring model (such as, bad scalability to device scale applications, poor distributed memory platform performance) due to which it has not found wide traction in the multiphase flow CFD community.

In the MPPIC model the collisions are not directly resolved. Unlike in the coarse-grain DEM model, since the physical volume of the parcels do not conserve the physical volume implied by real particles, the collisions in MPPIC model should ideally be based on mean fields (such as solid volume fraction), and their spatial gradients, that are computed from the parcels. Using the mean fields computed on the Eulerian grid is in fact the underlying philosophy/motivation behind the initial development of MPPIC model (Andrews and O'Rourke, 1996) wherein it is envisioned that in typical applications the number of Eulerian grid cells will be less than the number of tracked parcels; hence, the computational cost in MPPIC model will be comparable to two-fluid model while the extension to polydispersity will not result in numerical and modeling complications associated with two-fluid model. However, the estimation of mean fields from Lagrangian data is fraught with noise stemming (Xu and Pope, 1999) from statistical errors (due to finite sample size). As a result, it is not trivial to extend the closures used in two-fluid theory (based on mean fields and their spatial gradients) to model collisions in the MPPIC model. Before going into further details of collision modeling in MPPIC, the governing equations used to describe the motion of parcels are first discussed.

For the ease of discussion, the superscript i in front of Lagrangian variables is dropped hereinafter. The position and velocity of the i^{th} parcel evolve as

$$\frac{d\mathbf{X}_{\text{p}}(t)}{dt} = \mathbf{V}_{\text{p}}(t), \tag{5}$$

$$m_{\text{p}}\frac{d\mathbf{V}_{\text{p}}(t)}{dt} = m_{\text{p}}\mathbf{g} + \mathbf{F}_{\text{p,drag}}(t) + \mathbf{F}_{\text{p,coll}}(t), \tag{6}$$

where $m_{\text{p}} = \rho_{\text{p}}\dfrac{\pi D_{\text{p}}^3}{6}$ is mass of the parcel, $\mathbf{g}$ is the acceleration due to gravity, $\mathbf{F}_{\text{p,drag}}$ is the total drag force (pressure + viscous) acting on the parcel, $\mathbf{F}_{\text{p,coll}}$ is the force due to inter-particle collisions. Although from the above equations it might appear as if one parcel contains only one real particle (i.e., $W_{\text{p}} = 1$), it is not the case as a parcel consists of identical real particles that are assumed to experience identical forces; therefore, W_{p} falls out from both sides. The effect of multiple particles clumped together to form a parcel is manifested through solids volume fraction in the drag force term. The details of drag force and collision terms are discussed in the next two

subsections.

2.3 Particle-fluid interaction term $\mathbf{F}_{\mathrm{p,drag}}$

In the MFIX-PIC code, there are two options to compute the particle-drag force $\mathbf{F}_{\mathrm{p,drag}}$. In the first approach, the slip velocity is based on the cell centered average velocities for gas and solids phases. This approach results in equal drag force for all parcels residing in a particular grid cell. In the second approach, slip velocity is based on the gas-phase velocity interpolated at the parcel location and the instantaneous parcel velocity. The second approach is described below.

Consider i^{th} parcel, belonging to m^{th} solid–phase, that resides in k^{th} computational cell at time t. The drag force on this parcel is represented as

$$\mathbf{F}_{\mathrm{p,drag}} = -\boldsymbol{\nabla} P_{\mathrm{g},k} \mathcal{V}_{\mathrm{p}} + \frac{\beta_{\mathrm{m}} \mathcal{V}_{\mathrm{p}}}{\varepsilon_{sm}} \left(\mathbf{v}_{\mathrm{g}}(\mathbf{X}_{\mathrm{p}}) - \mathbf{V}_{\mathrm{p}} \right), \tag{7}$$

where $\boldsymbol{\nabla} P_{\mathrm{g},k}$ is the pressure gradient at the cell center of k^{th} grid cell, and $\mathbf{v}_{\mathrm{g}}(\mathbf{X}_{\mathrm{p}})$ is the gas-phase velocity $\mathbf{v}_{\mathrm{g}}$ field interpolated at the particle location, $\mathcal{V}_{\mathrm{p}} = \frac{\pi D_{\mathrm{p}}^3}{6}$ is the parcel volume, and β_{m} is the local gas-solid momentum transfer coefficient for a parcel residing in k^{th} cell. An explicit functional form of β_{m} is not known theoretically and, therefore, different correlations deduced from experimental and numerical studies are used to model this term.

The Eulerian drag force ($\mathbf{I}_{\mathrm{g}m}$ in the gas-phase momentum conservation equation 2) at k^{th} cell center (denoted by $\mathbf{x}_k$) is computed as

$$\mathbf{I}_{\mathrm{g}m}^{k} = \frac{1}{\mathcal{V}_{\mathrm{k}}} \sum_{i=1}^{N_{\mathrm{m}}} W_{\mathrm{p}}^{(i)} \mathbf{F}_{\mathrm{p,drag}}^{(i)} K(\mathbf{X}_{\mathrm{p}}^{(i)}, \mathbf{x}_k), \tag{8}$$

where $K(\mathbf{X}_{\mathrm{p}}^{(i)}, \mathbf{x}_k)$ is a generic kernel with compact support and determines the influence of the particle force at $\mathbf{X}_{\mathrm{m}}^{(i)}$ on a grid cell center located at $\mathbf{x}^k$, and $\mathcal{V}_{\mathrm{m}}$ is the geometric volume of the k^{th} grid cell.

2.4 Particle-particle interaction term $\mathbf{F}_{\mathrm{p,coll}}$

Following the same terminology used in discussion of closure models for solid stresses in two-fluid-model, the collisions in MPPIC model can be decomposed into viscous and frictional regimes. The viscous regime is characterized by binary collisions, while the frictional regime is characterized by enduring contacts. The initial MPPIC developments (Andrews and O'Rourke, 1996; Snider, 2001) modeled only the frictional stresses by expressing $\mathbf{F}_{\mathrm{p,coll}}$ as the gradient of the stress tensor with off-diagonal elements set to zero. The sole purpose of this resulting radial stress term was to prevent solids from packing over the theoretically allowed maximum value. Only very recently, viscous stresses have been implemented in MPPIC model by O'Rourke et al. (2009); O'Rourke and Snider (2010) which are based on Bhatnagar, Gross, and Krook (BGK) approximation to the collision terms in the evolution equation for particle distribution function. It was shown by O'Rourke and Snider (2010) that the inclusion of viscous stresses corrects some of the anomalies observed in the MPPIC model.

Although the viscous stress and its accurate modeling is critical to the fidelity of MPPIC model, it is not critical to its stability. From the perspective of solids phase, frictional stresses have the leading order effect on the stability of MPPIC model. If the frictional stresses are not able to prevent solids from packing over the close-packing limit, then the simulations become very unstable quickly

and eventually blow up. Due to the siginificance of frictional stresses on the stability of MPPIC model, this study is only limited to modeling frictional stresses under the $\mathbf{F}_{\text{p,coll}}$ term. Future studies will be devoted to the implementation of viscous stresses in the MFIX-PIC code.

Since the only available implementations of MPPIC model are commercial, it is not possible to fully verify the fine details of model implementation and one has to rely on the public domain information. In this regard, we discuss the numerical implementation of frictional stress as proposed by Snider (2001) along with noting the fact that the current implementation in the commercial code might be substantially different over years of more work.

3 Numerical implementation: past studies

For the frictional stress component in $\mathbf{F}_{\text{p,coll}}$, the force on the parcel is computed based on the following form for the stress tensor

$$\mathbf{F}_{\text{p,coll}} = -\frac{\mathcal{V}_{\text{p}}}{\varepsilon_{\text{s}}}\boldsymbol{\nabla}\tau, \tag{9}$$

where τ is an isotropic inter-particle stress whose off-diagonal elements are neglected. This continuum particle stress model is based on the original expression of Harris and Crighton (Harris and Crighton, 1994) modified to remove singularity at the close pack limit. It is given as

$$\tau = \frac{P_{\text{s}}\varepsilon_{\text{s}}^{\beta}}{\max\left[\varepsilon_{\text{s,cp}} - \varepsilon_{\text{s}}, \varepsilon\left(1-\varepsilon_{\text{s}}\right)\right]}, \tag{10}$$

where P_{s} has units of pressure and values between and 1 Pa and 100 Pa are recommended. $\varepsilon_{\text{s,cp}}$ is the close packing limit and its choice is also somewhat arbitrary as it depends on size, shape, and ordering of the particles. Typical choice for $\varepsilon_{\text{s,cp}}$ is 0.6. The constant β is also arbitrarily specified with recommended values in the range $2 \leq \beta \leq 5$ (Auzerais et al., 1988). ε is a small number on the order of 10^{-7} and it is added to remove the singularity at the close pack limit.

As will be discussed later, this stress term does not affect the particle stresses except when the solid volume fraction approaches or exceeds close pack. Even when that limit is reached, the above expression never explicitly enters any governing equations. It is used only as a guideline to decide the new velocity of a parcel approaching, exiting, or embedded in a close pack. Before further discussing how the above term is actually implemented, it becomes necessary to discuss the discretization of the particle governing equations 5 and 6 as proposed by Snider (2001).

Parcel's position is updated as

$$\mathbf{X}_{\text{p}}^{n+1} = \mathbf{X}_{\text{p}}^{n} + \Delta t\mathbf{V}_{\text{p}}^{n+1}, \tag{11}$$

where Δt is the solids time-step size. The parcel's velocity at $n+1$ does not follow directly from the governing equation 6. The new velocity $\mathbf{V}_{\text{p}}^{n+1}$ is decomposed as

$$\mathbf{V}_{\text{p}}^{n+1} = \widetilde{\mathbf{V}}_{\text{p}} + \mathbf{V}_{\text{p}\tau}, \tag{12}$$

where $\widetilde{\mathbf{V}}_{\text{p}}$ is an intermediate parcel velocity obtained by neglecting the $\mathbf{F}_{\text{p,coll}}$ term in equation 6. It is given as

$$\widetilde{\mathbf{V}}_{\text{p}} = \mathbf{V}_{\text{p}}^{n} + \left(\frac{\mathbf{F}_{\text{p,drag}}^{n+1}}{m_{\text{p}}} + \mathbf{g}\right)\Delta t. \tag{13}$$

It should be noted that if the solids velocity in the $\mathbf{F}_{\text{p,drag}}$ expression in equation 7 is written at time n when expanded above, then that will reduce the above discretization to the exact implicit

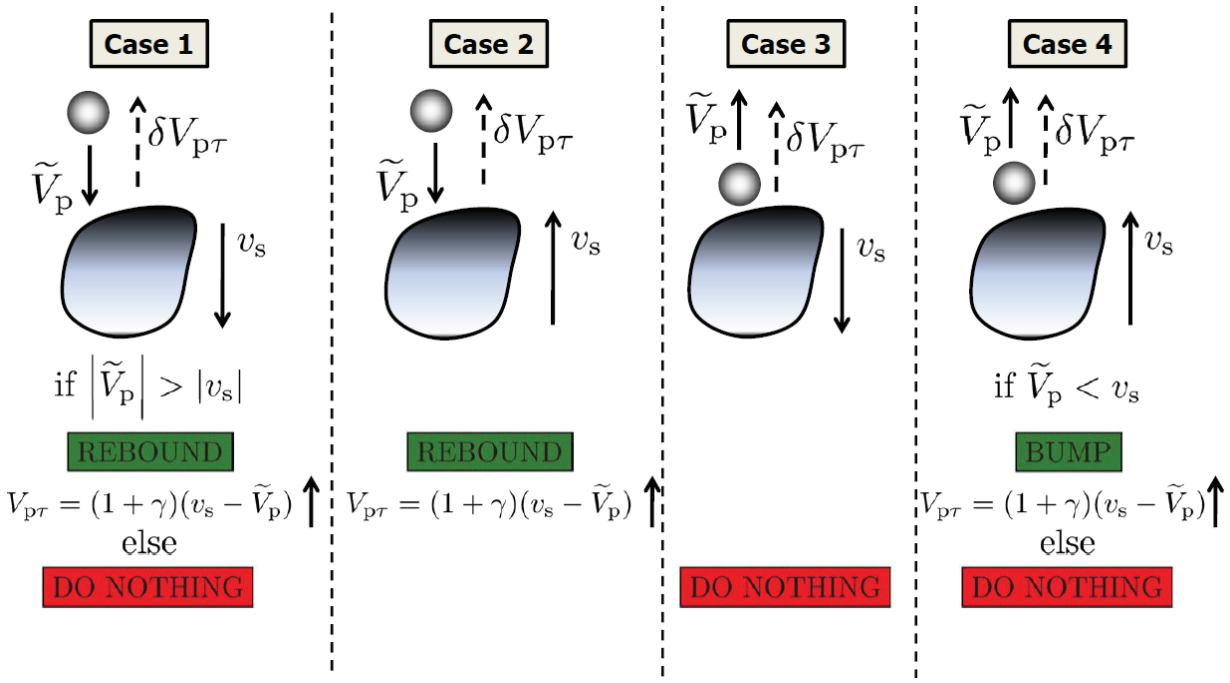

Figure 2: A schematic showing the four cases that result from the limiter in Snider's frictional model described by equation 15. The analysis is limited to vertical direction and also $\boldsymbol{\nabla}\tau < 0$, such that the direction of impulse velocity is positive, i.e., $\delta V_{p\tau} > 0$.

expression in Snider (2001). The frictional stress is implemented through $\mathbf{V}_{p\tau}$ in the decomposition of $\mathbf{V}_p^{n+1}$ in equation 12.

Since the other component of velocity $\mathbf{V}_{p\tau}$ in equation 12 is due to the interaction of a parcel with a close pack, it can be thought of as velocity correction due to an impulse imparted during a collision; hence, $\mathbf{V}_{p\tau}$ will be referred to as "impulse velocity". The first step in calculation of $\mathbf{V}_{p\tau}$ is the estimation of an intermediate impulse velocity as

$$\delta\mathbf{V}_{p\tau} = -\frac{\Delta\tau}{\rho_p \varepsilon_s \left(1 + \frac{\beta\Delta t}{\rho_p \varepsilon_s}\right)}. \tag{14}$$

Since the solid stress τ (Eq. 10) becomes significant only when ε_s values approach or exceed close-pack, the above impulse velocity is orders of magnitude lower than $\widetilde{\mathbf{V}}_p$ in other regions of the flow. Furthermore, since $\delta\mathbf{V}_{p\tau}$ is calculated based on the spatial derivatives of solids volume fraction which is itself computed from finite particles, the numerical estimation of impulse velocity suffers from very large statistical errors (Garg et al., 2006). As a thought process, a uniform particle distribution can result in significant finite values for $\delta\mathbf{V}_{p\tau}$ and the typical distributions encountered in multiphase flows are far from being uniform; especially in steep gradient (with respect to solid volume fraction) regions near close pack where the frictional stresses will be most active. In regions of close-pack, the above expression will yield extremely large (due to near singularity there) impulse velocity, resulting in unrealizable ballistic particle trajectories.

Due to the aforementioned reasons, the impulse velocity in equation 14 is never used as is. However, it is used in conjunction with limiters which are described below. Limiting our attention only to $k-$ direction having unit vector $\mathbf{e}_k$, if $(\boldsymbol{\nabla}\tau)\cdot\mathbf{e}_k < 0$, then $V_{p\tau_k}$ (impulse velocity in the $k-$

direction) in equation 12 is computed as

$$\begin{aligned}
&(\boldsymbol{\nabla}\tau)\cdot\mathbf{e}_k < 0,\\
&\quad V'_{\mathrm{p}\tau_k} = \min\left(\mathbf{e}_k\cdot\delta\mathbf{V}_{\mathrm{p}\tau},\,(1+\gamma)\left(\mathbf{v}_{\mathrm{s}}-\widetilde{\mathbf{V}}_{\mathrm{p}}\right)\cdot\mathbf{e}_k\right),\\
&\quad V_{\mathrm{p}\tau_k} = \max\left(V'_{\mathrm{p}\tau_k},0\right),
\end{aligned} \tag{15}$$

where γ is related to coefficient of restitution, and $\mathbf{v}_{\mathrm{s}}$ is the mean solids velocity which could be average solids velocity at the cell center or average solids velocity interpolated at the parcels position. Although at first glance the above limiters appear complicated and also do not appear to be based on any physical rationales, it is not the case. For the ease of explanation, if the attention is limited to vertical direction and $\boldsymbol{\nabla}\tau < 0$ (such that $\delta V_{\mathrm{p}\tau} > 0$ in this direction), then, as shown by the schematic in figure 2, the above limiter breaks down into four cases:

- *Case 1, both parcel and the close pack moving down.* If the parcel's intermediate velocity magnitude $\left|\widetilde{V}_{\mathrm{p}}\right|$ is higher than the magnitude of the solids mean velocity $|v_{\mathrm{s}}|$, then the parcel's impulse velocity $V_{\mathrm{p}\tau}$ will be in the direction opposite (up, in this case) to its approach velocity $\widetilde{V}_{\mathrm{p}}$, and from the limiter above it will be $V_{\mathrm{p}\tau} = (1+\gamma)\left(v_{\mathrm{s}}-\widetilde{V}_{\mathrm{p}}\right)$. Substituting this $V_{\mathrm{p}\tau}$ in equation 12, and upon rearranging the terms, the parcel's final velocity at V_{p}^{n+1} becomes

$$V_{\mathrm{p}}^{n+1} = v_{\mathrm{s}} - \gamma\left(\widetilde{V}_{\mathrm{p}} - v_{\mathrm{s}}\right) \tag{16}$$

  Depending on the magnitude of relative velocity ($\left(\widetilde{V}_{\mathrm{p}} - v_{\mathrm{s}}\right)$ in the above equation), the parcel's final velocity V_{p}^{n+1} might be reflected or the parcel might keep moving downwards with a reduced speed.

- *Case 2, parcel and the close pack are moving in opposite directions but approaching*: The parcel's impulse velocity $\widetilde{V}_{\mathrm{p}}$ will be in the direction opposite to its approach velocity $\widetilde{V}_{\mathrm{p}}$. The parcel's final velocity V_{p}^{n+1} takes the same form as derived for case 1 in equation 16; however, unlike in case 1, for this case the parcel's final velocity V_{p}^{n+1} will definitely be in the direction opposite to the approach velocity $\widetilde{V}_{\mathrm{p}}$.

- *Case 3, parcel and close pack moving in opposite directions but separating*: No action is needed here as the parcel and close pack are not on a collision path.

- *Case 4, both parcel and the close pack moving up*: This is similar to case 1, except that here the parcel receives a bump if its speed is lower than the speed of the close pack that is coming from behind. The parcel's impulse velocity $V_{\mathrm{p}\tau}$ and final velocity V_{p}^{n+1} take the same form as noted in case 1.

Similar analysis can be done for the other case of $\boldsymbol{\nabla}\tau < 0$. The above analysis could also be done with the aid of relative velocity. If the relative velocity of parcel with respect to close pack is defined as $\mathbf{V}_{\mathrm{rel}} = \widetilde{\mathbf{V}}_{\mathrm{p}} - \mathbf{v}_{\mathrm{s}}$, then if $\mathbf{V}_{\mathrm{rel}}\cdot(-\boldsymbol{\nabla}\tau) < 0$ (i.e., the relative velocity and impulse force from collision are in the opposite direction), the parcel's relative velocity is reflected (to $-\gamma\mathbf{V}_{\mathrm{rel}}$) and its final velocity $\mathbf{V}_{\mathrm{p}}^{n+1}$ becomes

$$\mathbf{V}_{\mathrm{p}}^{n+1} = \mathbf{v}_{\mathrm{s}} - \gamma\mathbf{V}_{\mathrm{rel}}; \quad \text{if} \quad \mathbf{V}_{\mathrm{rel}}\cdot(-\boldsymbol{\nabla}\tau) < 0. \tag{17}$$

On substituting for $\mathbf{V}_{\mathrm{rel}}$, the above expression becomes identical to expression derived in equation 16 from the limiters and incorporates all four cases discussed above.

From the above discussion of frictional stresses, it is clear that the exact form of stress tensor does not matter. It is like a coloring function and its sole use is to provide guidance. The final outcome in terms of parcel's velocity on interaction with close-pack is based on simple rules that become very intuitive on assuming the close pack to be of infinite mass or to be a wall. In regions of flow where close packing is not encountered, the correction due to impulse velocity $\mathbf{V}_{\mathrm{p}\tau}$ is orders of magnitude less than the intermediate velocity $\widetilde{\mathbf{V}}_{\mathrm{p}}$, so again the form of stress tensor does not matter.

In our first implementation of the frictional stress model as described above, we observed onset of severe instabilities as the solver was not able to maintain close packing in flows such as sedimentation. We believe it is due to additional rules that are used in conjunction to the limiter described above. For example, the parcel's maximum displacement is possibly limited based on mean free path. However, due to the commercial nature of existing MPPIC model implementations, it is not possible to verify any additional rules that have not been mathematically formulated or documented in archived journals. In the next section, we discuss the frictional stress term that has been implemented in the MFIX-PIC code.

4 Numerical implementation: current study

The MPPIC model development in this study was guided by simulating three different physical problems that encompass the physical phenomena observed in typical applications of gas-solids flows. The first problem is the particle sedimentation problem where an initially dilute suspension is allowed to fall under gravity and settle as close-pack. The other two setups are for central jet fluidized bed and uniformly fluidized bed. The final MPPIC model should be robust enough to handle all three applications and at the same time capable of capturing disparate physical phenomena taking place in these there physical problems. In the following discussion, we discuss the implementation of MPPIC model in MFIX and how the development evolved (or fine tuned) based on the feedback from applying the model concurrently to the three problems.

Our implementation is nearly identical to the one proposed in Snider (2001) except for the form of stress tensor and adjustments to the four cases (see the schematic in Fig. 2) discussed earlier. These adjustments have been made so as to make the solver stable. The discretized forms of the parcel's governing equations 5 and 6 are identical to the expressions in equations 11 and 12. Based on our observation that the exact form of stress tensor does not matter, we use a coloring function χ to implement the frictional stresses. The coloring function is defined as

$$\begin{aligned} \chi &= \varepsilon_{\mathrm{s}} \quad \varepsilon_{\mathrm{s}} \geq \varepsilon_{\mathrm{s,cp}}\,, \\ &= 0 \quad \text{otherwise}\,. \end{aligned} \tag{18}$$

Using the same convention as used in previous section, the direction of the impulse velocity $\delta\mathbf{V}_{\mathrm{p}\tau}$ is calculated as

$$\delta\mathbf{V}_{\mathrm{p}\tau} = -\boldsymbol{\nabla}\chi. \tag{19}$$

$\delta\mathbf{V}_{\mathrm{p}\tau}$ serves the same purpose as the intermediate impulse velocity calculated in equation 14 for Snider's frictional model of specifying the direction of the final impulse velocity $\mathbf{V}_{\mathrm{p}\tau}$. Limiting attention to motion in the vertical direction, once again four cases arise that were shown earlier by the schematic in figure 2. In the current implementation, if the relative velocity of parcel with respect to the close pack ($\mathbf{V}_{\mathrm{rel}} = \widetilde{\mathbf{V}}_{\mathrm{p}} - \mathbf{v}_{\mathrm{s}}$) is found to be approaching the close pack (i.e., $\mathbf{V}_{\mathrm{rel}} \cdot (\delta\mathbf{V}_{\mathrm{p}\tau}) < 0$), then the relative velocity is reflected and the parcel's final velocity $\mathbf{V}_{\mathrm{p}}^{n+1}$ at $n+1$ is calculated as

$$\mathbf{V}_{\mathrm{p}}^{n+1} = \mathbf{v}_{\mathrm{s}} - e_1^{\mathrm{fric}}\mathbf{V}_{\mathrm{rel}}; \quad \text{if} \quad \mathbf{V}_{\mathrm{rel}} \cdot (\delta\mathbf{V}_{\mathrm{p}\tau}) < 0, \tag{20}$$

where e_1^{fric} is some kind coefficient of restitution in the frictional regime and a different symbol is used to denote it here compared to the symbol γ used in Snider's model in order to differentiate the two models. Plugging the expression for relative velocity in the above equation, it can be seen that the above is identical to that derived earlier (Eq. 17) for Snider's frictional model.

On simulating the sedimentation problem (first of the three problems identified above) using Snider's and the newly proposed frictional stress models as is, the simulations were found to be very unstable and were unable to prevent solid packings going over the theoretical limits and would ultimately end up with solids occupying more than 100% of physical volume (i.e., negative gas voidage). Through some trial and error, it was found that an adjustment to case 1 in figure 2 resulted in unconditionally stable simulations for the sedimentation problem. According to this adjustment, if a parcel encounters a close-pack while moving in the direction of gravity force and its speed is higher than the mean speed of the close-pack (i.e, $\left|\widetilde{V}_{\text{p}}\right| > |v_{\text{s}}|$), then it is always reflected. If the gravity is in the negative $y-$ direction, then this scenario corresponds to case 1 in figure 2. Note that according to frictional stress model implied by equation 20 above, the direction of parcel's final velocity $\mathbf{V}_{\text{p}}^{n+1}$ depends on the magnitude of the relative velocity. As a result, the parcel's final velocity will either be reversed or it will slow down. However, if the parcel's final velocity is always reflected as

$$V_{\text{p}}^{n+1} = -e_1^{\text{fric}}\widetilde{V}_{\text{p}}, \tag{21}$$

then the simulation of sedimentation problem becomes unconditionally stable.

It should be noted that the above adjustment applies only when the parcel is moving vertically downwards in the direction of gravity and encounters a close pack. Analogously, a parcel can be moving vertically upwards and encounter a close-pack that will again correspond to Case 1 in figure 2, except that in this case the impulse velocity direction will be in direction opposite (i.e., $\delta V_{\text{p}\tau} < 0$) to that shown in figure 2. On extending the above adjustment to this direction, it was found that although the MPPIC simulations were very stable, they also resulted in nearly frigid bed (very less movement of particles) conditions for fluidized bed applications where the system is known/expected to fluidize for the chosen operating conditions. It was observed that bed would attain an initial configuration beyond which the parcels would not move much. Therefore, the adjustment in equation 21 is only limited to conditions noted above with it. This adjustment can be written more formally as

$$V_{\text{p},k}^{n+1} = -e_1^{\text{fric}}\widetilde{V}_{\text{p},k}, \quad \text{if } \delta\mathbf{V}_{\text{p}\tau}\cdot(g\mathbf{e}_k) < 0, \text{ and } \widetilde{\mathbf{V}}_{\text{p}}\cdot(g\mathbf{e}_k) > 0, \tag{22}$$

where $\mathbf{e}_k$ is the direction of the gravity force. This special adjustment will be referred to as "Case 1a".

Although the adjustment for gravity to the frictional stress model by Case 1a results in unconditionally stable simulations for the sedimentation problem, the fluidized bed applications were still found to suffer from onset of instabilities from over packing of solids in few cells in the domain. On further trial and error, it was found that upon yet one more adjustment to case 1 in figure 2 resulted in unconditionally stable simulations for all applications considered in this study. According to equation 20, a parcel's velocity for case 1 in figure 2 gets reflected only when its speed is higher than the mean speed of the close-pack (i.e., $\left|\widetilde{V}_{\text{p}}\right| > |v_{\text{s}}|$). However, a parcel on colliding with a close-pack should ideally loose some momentum. Therefore, according to this new adjustment which will be referred as Case 1b, even if a parcel's speed is less than the mean speed of close-pack (i.e., $\left|\widetilde{V}_{\text{p}}\right| < |v_{\text{s}}|$) for case 1 in figure 2, then, rather then doing nothing (i.e., $V_{\text{p}}^{n+1} = \widetilde{V}_{\text{p}}$), its final velocity V_{p}^{n+1} is calculated as

$$V_{\text{p}}^{n+1} = e_2^{\text{fric}}\widetilde{V}_{\text{p}}, \tag{23}$$

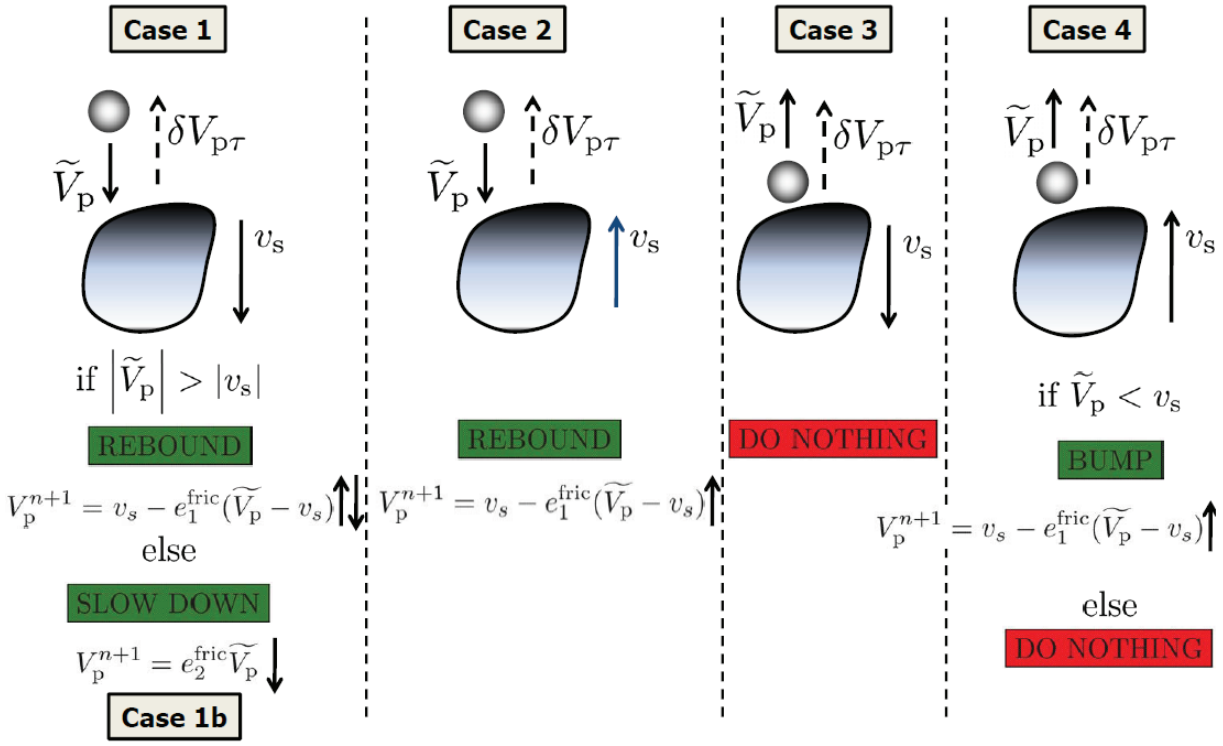

Figure 3: A schematic showing cases 1-4 along with case 1b used to define frictional stress model in the current study. It is noted that the complete frictional stress model also consists of Case 1a (Eqn 22) which is a special adjustment to Case 1 in the direction of gravity. Due to the generic nature of the above schematic, this special Case 1a is not shown here.

where e_2^{fric} is a new parameter and is different from e_1^{fric} so far used in the current frictional stress model. It was found that values in the range $0.9 - 0.95$ for e_2^{fric} resulted in unconditionally stable simulations. The above two frictional coefficients of restitution (e_1^{fric} and e_2^{fric}) are set by the flags "MPPIC_COEFF_EN1" and "MPPIC_COEFF_EN2", respectively, through the MFIX input file.

5 Computational Details

In this section, a short overview of the computational implementation of the above MPPIC model in MFIX-PIC code is given. This should serve as a starting point for understanding the numerical methods, code structure, and implementation. A more detailed Doxygen output in the pdf and html formats can be downloaded from the MFIX website for those who wish to dig deeper into the code. Below is the algorithm implemented in MFIX-PIC.

1: Read initial gas flow field, parcel positions and velocities, boundary conditions etc.: This is done through *mfix* calling *get_data* subroutine. *get_data* in turns calls *init_namelist/des_init_namelist*, *des_allocate_arrays*, and *des_init_arrays*. In addition, *des_check_data* is called to perform some sanity checks.

2: Compute values at next time step: mfix calls *time_march* to compute the gas phase quantities at the next time step. *Time_march* in turn calls *des_time_march* which calls *mppic_time_march* to calculate the updated values for the particles through the following iteration

3: *mppic_time_march* is called which calls several other routines listed below:

call *compute_pg_grad* to determine the gas-phase pressure gradient field. This is done at the outer loop of solid phase time stepping since gas-phase pressure gradient remains constant during the call to *mppic_time_march*

call *particles_in_cell* to determine the parcel location on the background Eulerian grid. Within the same routine, dispersed phase mean fields, such as solid volume fraction and average solid velocities, are estimated by default second-order Lagrange polynomial interpolation. Estimation of solid volume fraction by interpolation (as opposed to simple arithmetic averaging) is critical to the stability of the MPPIC model. Therefore, estimation by interpolation is set to default in MPPIC model. The interpolation details can be found in Garg et al. (2011).

call *mppic_compute_ps_grad* to compute the coloring function and the resulting direction of the impulse velocity $\delta\mathbf{V}_{\mathrm{p}\tau}$ (Eqns. 18 and 19) on the Eulerian field. For the purpose of implementing the actual frictional stress model, the impulse velocity direction field is interpolated on to the parcel's location. Therefore, within the same routine, using the default second order Lagrange polynomial interpolation, the impulse velocity direction field $\delta\mathbf{V}_{\mathrm{p}\tau}(\mathbf{x})$ is forward interpolated to the parcel's location at $\mathbf{X}_{\mathrm{p}}$. Along with the forward interpolation of $\delta\mathbf{V}_{\mathrm{p}\tau}(\mathbf{x})$, the solid's phase mean velocity field is also interpolated to the parcel's location. Therefore, any reference to $\mathbf{v}_{\mathrm{s}}$ in Eqns. 18 through 23 describing the frictional stress model in MFIX-PIC code implies interpolated solids phase mean velocity field.

call *calc_des_drag_gs* to compute the drag force acting on the parcels. If the flag "DES_INTERP_ON" is True, then the drag force on parcels is obtained by forward interpolation of the gas-phase velocity field, and the drag force on the Eulerian grid is obtained by backward interpolation of individual drag force on parcels. If the flag "DES_INTERP_ON" is False, then the drag force is first obtained on the Eulerian grid based on Eulerian fields for solids volume fraction, and also solids and gas phase velocity fields. It is noted that in MPPIC model the solids phase mean fields are always estimated from backward interpolation in earlier call to *particles_in_cell* routine. This Eulerian drag force is then equally distributed among the parcels residing in that cell.

cfupdateold to update the parcels' attributes from the previous time step to the latest time step.

cfnewvalues based on the information from all these routines to compute new attributes for parcels, such as position, velocity, etc. As discussed earlier, the time-step integration is decomposed into two-steps wherein. During the first step, an intermediate parcel velocity $\widetilde{\mathbf{V}}_{\mathrm{p}}$ is obtained by taking into account all external forces except inter-particle interactions. Among the inter-particle interactions, the most critical (stability wise) frictional stress forces are applied during the second step following the numerical implementation laid out in section 4. It is again noted here that the impulse velocity direction $\delta\mathbf{V}_{\mathrm{p}\tau}$ and solids phase mean velocity $\mathbf{v}_{\mathrm{s}}$ referenced in equations describing the numerical implementation of frictional stress model in MFIX-PIC are first forward interpolated at parcels location during the earlier call to routine *mppic_compute_ps_grad*.

call *mppic_apply_wallbc* to reflect the out of bound parcels back into the physical domain. The parcels undergo a purely specular reflection. The normal component of the particles approach velocity is restituted. This normal coefficient of restitution is set by the flag "MPPIC_COEFF_EN_WALL" in MFIX input file.

4: Iterate in mppic_time_march till $\Sigma\Delta t_{\rm sol} = \Delta t_{\rm gas}$
5: Iterate in time_march till $\Sigma\Delta t_{\rm sol} \geqslant t_{\rm write}, t_{\rm restart}$, etc.
6: Iterate in time_march till $\Sigma\Delta t_{\rm gas} \geqslant t_{\rm stop}$

We do not delve into the details of the numerical methods employed for the continuum part of the MFIX–DEM as they are widely covered elsewhere (Syamlal, 1998). Time-step size $\Delta t_{\rm sol}$ for the solid phase is calculated based on a CFL criteria and particle response time. It is computed as

$$\Delta t_{\rm sol} = \min\left\{\min\left\{\frac{\mathrm{CFL} * \Delta_i}{|V_{{\rm p},i}|}, i = 1,2,3\right\}, \Delta t_{\rm gas}, \Delta t_{\rm fac}\tau_{\rm sol}\right\}, \tag{24}$$

where $\Delta t_{\rm gas}$ is the time-step size used to evolve the gas-phase continuum fields, $\tau_{\rm sol} = \dfrac{\rho_{\rm p} D_{\rm p}^2}{18\mu_{\rm g}}$ is the particle response time, and $\Delta t_{\rm fac}$ is a user-defined pre-factor, defined by flag "DTSOLID_FACTOR" in the MFIX input file.

6 Results

Although the MPPIC model development was guided by simulating sedimentation and fluidized bed problems, the MPPIC model results for sedimentation problem will not be discussed here. This is because the critical issue in sedimentation problem was the ability of MPPIC model to sustain close packing. The addition of case 1a (Eq. 22) to frictional stress model (Eq. 20) results in unconditional stability for the sedimentation problem. Beyond this, there is not much with regard to quantitative data that can be compared. We will focus our attention on the central jet fluidized bed problem that had proven to be most challenging to simulate using MPPIC model. We will discuss the sensitivity of simulation results choices made for the frictional stress model. The MPPIC model results will be compared to the more accurate DEM results. The next section describes the physical problem setup.

6.1 Problem setup

The first test problem is based on experimental investigations of the bubble formation at a jet within a fluidized bed by Kuipers (1990). The experiments were carried out on a shallow test rig that is 57 cm wide, 100 cm tall, and 1.5 cm deep (shown by Fig. 4). As shown by the schematic in Fig. 4, a jet with an outlet velocity of 10 cm/s and 1.5 cm wide is introduced at the geometrical center of the bottom face. The rest of the bed is fluidized with its minimum fluidization velocity of 0.25 m/s. The bed is filled up to a height of 0.5 m with glass beads of diameter 500 μm and density 2660 Kg/m^3.

In the numerical simulations, the bed is discretized uniformly by $15,200$ grid cells that are 0.75 cm wide, 1 cm tall, and 0.75 cm thick. This grid prescription is based on previous numerical studies (Boemer et al., 1997; Patil et al., 2005) that indicate a grid independent solution at this resolution. The MFIX-PIC simulations will be compared with the Eulerian-Eulerian simulations performed using MFIX. They will also be compared with the commercial implementation of MPPIC model in CPFD's software Barracuda. To closely mimic the experimental conditions, the bed is initialized up to a bed height of 50 cm with spherical particles of diameter 500 μm and density

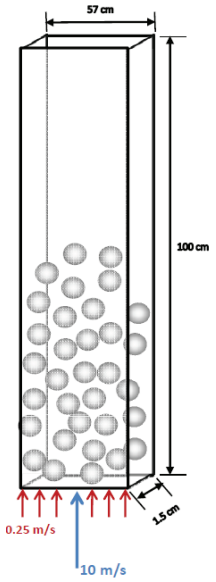

Figure 4: Schematic illustration of the central jet fluidized bed setup.

2660 Kg/m^3. Initial solids volume fraction is set at 0.6, resulting in initial inventory of 6.82 Kg. This solids inventory implies a total of nearly 40 million particles due to which the DEM simulations of this system become prohibitive.

Some of the critical numerical parameters in MFIX-PIC simulations are statistical weight W, the frictional coefficient's of restitution e_1^{fric}, e_2^{fric}, minimum gas voidage $\varepsilon_{\text{g,min}}$, and nominal number of parcels per cell N_{pc}^n [1]. First a baseline set up will be defined for MFIX-PIC simulations which will be used to compare with MFIX-TFM and CPFD simulations. In the baseline set up, the solids loading is uniformly represented by 5 parcels per cell (i.e., initially $N_{\text{pc}}^n = 5$) for a total of $38,000$ ($=5 \times 76 \times 50 \times 2$) parcels. Since the actual number of real particles if tracked individually for this system is nearly 40 million, this implies that the statistical weight W or the number of real particles represented by each parcel is approximately $1,000$. This value for statistical weight will be later varied in order to study its sensitivity. Minimum gas voidage is set to 0.38. In the baseline set up, both the frictional coefficients of restitution are set to 0.5 and their sensitivity will also be studied later. Particles are specularly reflected at the walls with normal coefficient of restitution equal to 0.5.

For the CPFD simulations, Barracuda version 15.1 is used. To specify the friction stress model given by Eq. 10, P_{s} is set to 1, β is set to 3, and ε is set to 10^{-08}. Minimum gas voidage is again set to 0.38. Diffuse bounce is 0, and normal-to-wall and tangent-to-wall momentum retention values are set to 0.3 and 0.99, respectively. For the initial solids loading, approximately 5 parcels per cell are randomly seeded. For both MFIX-PIC and CPFD simulations, the top pressure outlet wall is set as a wall for solid phase in order to prevent random parcels from exiting the domain.

For the MFIX-TFM simulations, algebraic form of granular energy is used. No slip boundary conditions are applied for both gas and solid phases at the walls. For all MFIX based simulations, second order discretization is used for all variables and an outer iteration tolerance residue of 10^{-03}

[1] The nominal number of parcels per cell N_{pc}^n is defined as the total number of parcels by the total number of cells with non-zero solids volume fraction.

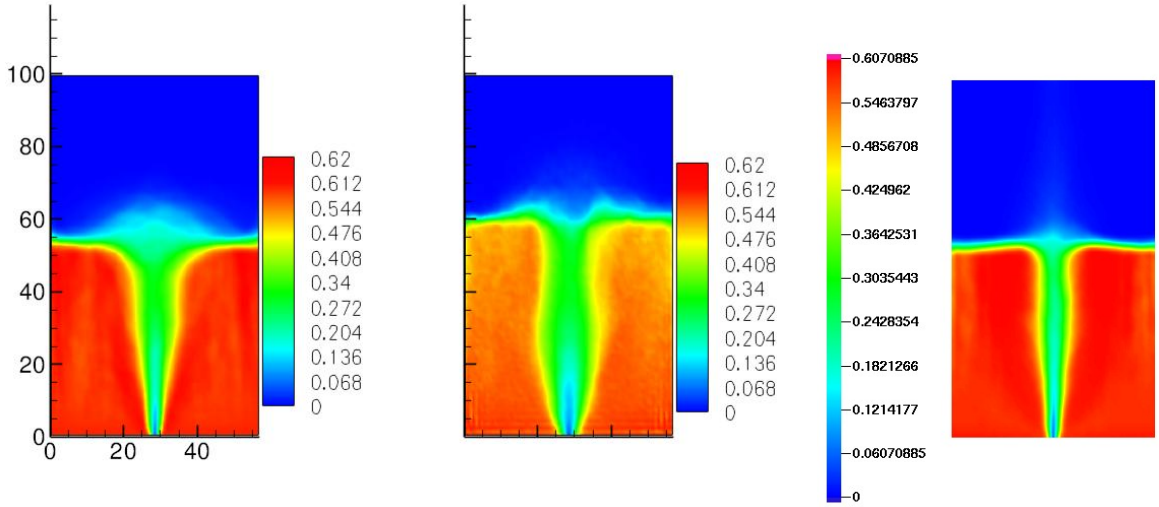

(a) MFIX-TFM (b) MFIX-PIC (c) CPFD

Figure 5: Comparison of time-averaged solid volume fraction profiles obtained from (a) MFIX-TFM, (b) MFIX-PIC, and (c) CPFD simulations.

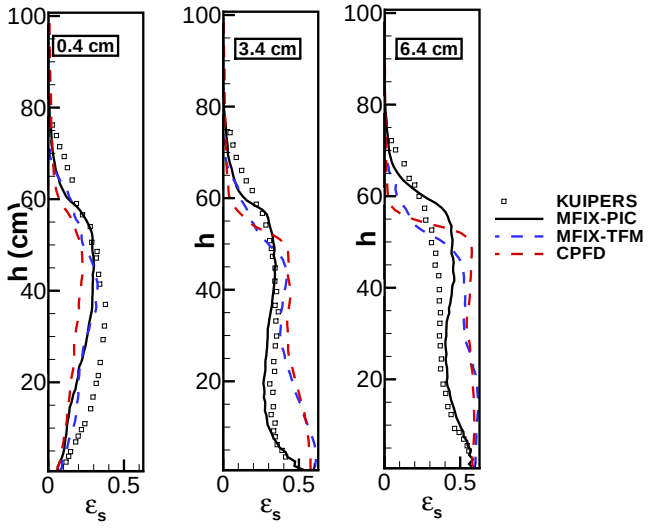

Figure 6: Comparison of time-averaged axial solid volume fraction profiles at different radial distances from the center.

is specified. Gidaspow drag law is used in all simulations (MFIX and CPFD). The problem is simulated for 30 seconds. The time averaged profiles are obtained for the last 10 seconds. Fig 5 shows the comparison of time-average contour plots of solid volume fraction obtained from MFIX-TFM, MFIX-PIC, and CPFD simulations. It can be seen that MFIX-PIC predicts overall lower solids volume fraction on either side of the central jet. As a result the average bed expansion is higher from MFIX-PIC and, at the same time, the zone of influence from central jet is larger. CPFD predicts the smallest zone of influence from central jet.

Fig. 6 shows the comparison of time averaged axial solid volume fraction profiles at different radial distances from center obtained from MFIX-PIC, MFIX-TFM, and CPFD simulations. Also shown in the same plots is the experimental data obtained by Kuipers (1990). From the plot it can be seen that the MPPIC model implemented in MFIX-PIC is in very good agreement with the experimental results for all radial distances from the jet. For radial distances equal to 3.4 cm and 6.4 cm and up to height equal to 40 cm, MFIX-TFM and CPFD predict higher solid volume fraction than MFIX-PIC which is consistent with the lower bed expansion observed earlier for MFIX-TFM and CPFD simulations from time averaged profiles of solid volume fraction in Fig 5. The results obtained from Eulerian-Eulerian simulation (MFIX-TFM) is consistent with results obtained from past numerical studies using continuum representation (Boemer et al., 1997).

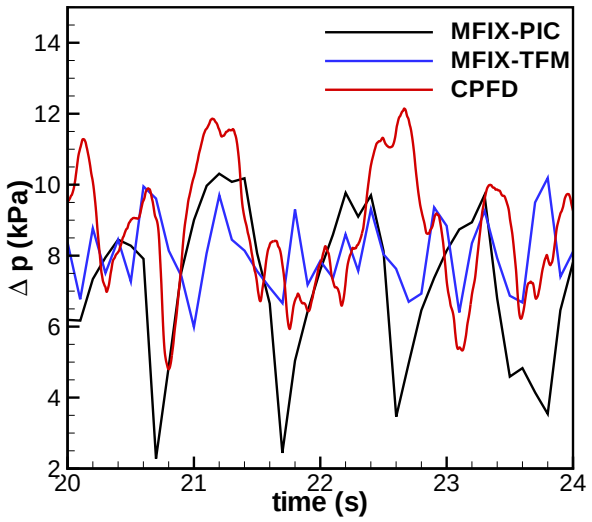

Figure 7: Pressure drop across the bed versus time for the Kuipers jet case obtained from MFIX-PIC, MFIX-TFM, and CPFD simulations.

Figure 7 shows the comparison the pressure drop across the bed obtained from MFIX-PIC, MFIX-TFM, and CPFD simulations. For the purpose of calculating pressure drop, the pressure at the outlet is assumed to be equal to atmospheric pressure (1 kPa). For MFIX-PIC and MFIX-TFM simulations, pressure at the base is computed by volume averaging the pressure field in the first row of physical cells. For CPFD simulation, pressure at the base is equal to the pressure in the bottommost cell next to the wall. It can be seen from the figure that on MFIX-TFM and CPFD yield nearly same pressure drop, while MFIX-PIC under-predicts the pressure drop. Both MFIX-PIC and CPFD simulations predict larger amplitude for pressure drop variation. Although not shown here, the bubble frequency from MFIX-PIC and CPFD simulations are in agreement with

each other but different from that obtained from MFIX-TFM simulation.

7 Remarks

The under-prediction of pressure drop by MFIX-PIC code is a cause of concern. The same under-prediction is observed for uniformly fluidized case where it is expected that the pressure drop should balance the weight of the suspended solids. The current implementation of MPPIC model has been found to be very stable. The users are encouraged to look at the implementation of MPPIC model in the MFIX-PIC code and report back fixes/improvements that can resolve the discrepancy around under-prediction of pressure drop.

The open-source implementation of MPPIC model provides the research community not only an under-the-hood insight of the MPPIC model, but it also provides a great avenue to enhance the model by improving the current physical model and/or adding new physical models that can improve the fidelity and also help with broader acceptance of MPPIC model. The current implementation is a first step toward better understanding of MPPIC model and below we identify some of the areas where the user community could start implementing their own models and make them part of the open-source MFIX CVS repository. Some possible ideas are

Viscous collision model: In the current implementation of interparticle interaction term $\mathbf{F}_{\mathrm{p,coll}}$, only the interactions in the frictional regime are accounted to prevent unphysical solids packing. There is a need to supplement the current model with interactions in the viscous regime. The users are encouraged to implement their own viscous stress models that can be updated to the MFIX CVS repository upon their consent;

Extension to cut-cell: MFIX code handles complicated geometries through recent cut-cell implementation. Although the MPPIC model will work with cut-cell, it has not been thoroughly tested and needs more development and testing to ensure conservative interphase coupling;

Parallel version: The current MPPIC model has been tested on serial compilation only. The existing DEM implementation should work with MPPIC as well; however, it has not been thoroughly tested;

polydispersity: The current frictional stress model has been tested for single phase only. Although the extension to polydispersity should not pose issues, the same has not been tested thoroughly. Users are encouraged to test the model and report back bugs and, if possible, fixes.

Two tutorials have been added to the MFIX CVS repository under the folder "$MFIX_HOME/tutorials/MPPIC_TUTORIALS/". The first tutorial is a setup for the Kuper's jet set up that is discussed in this documentation. The second tutorial is a set up of uniform fluidization.

8 MFIX-PIC user input variables

The MPPIC model User-Input variables needed to set up a MFIX-PIC simulation can be found in the common MFIX readme file found on the MFIX webpage at the following link
`https://mfix.netl.doe.gov/documentation/Readme.pdf`

9 Disclaimer

This report was prepared as an account of work sponsored by an agency of the United States Government. Neither the United States Government nor any agency thereof, nor any of their employees, makes any warranty, express or implied, or assumes any legal liability or responsibility for the accuracy, completeness, or usefulness of any information, apparatus, product, or process disclosed, or represents that its use would not infringe privately owned rights. Reference herein to any specific commercial product, process, or service by trade name,trademark, manufacturer, or otherwise does not necessarily constitute or imply its endorsement, recommendation, or favoring by the United States Government or any agency thereof. The views and opinions of authors expressed herein do not necessarily state or reflect those of the United States Government or any agency thereof.

References

Andrews, M., O'Rourke, P., 1996. The multiphase particle-in-cell (mp-pic) method for dense particulate flows. International Journal of Multiphase Flow 22 (2), 379 – 402.
URL http://www.sciencedirect.com/science/article/pii/0301932295000720

Auzerais, F. M., Jackson, R., Russel, W. B., 1988. The resolution of shocks and the effects of compressible sediments in transient settling. Journal of Fluid Mechanics 195, 437–462.
URL http://dx.doi.org/10.1017/S0022112088002472

Boemer, A., Qi, H., Renz, U., 1997. Eulerian simulation of bubble formation at a jet in a two-dimensional fluidized bed. International Journal of Multiphase Flow 23 (5), 927 – 944.
URL http://www.sciencedirect.com/science/article/pii/S0301932297000189

Cundall, P. A., Strack, O. D. L., 1978. The Distinct Element Method as a Tool for Research in Granular Media. Tech. Rep. NSF Grant ENG76-20711, National Science Foundation.

Garg, R., Galvin, J., Li, T., Pannala, S., 2011. Open-source mfix-dem software for gassolids flows: Part iverification studies. Powder Technology (0), –.
URL http://www.sciencedirect.com/science/article/pii/S003259101100502X

Garg, R., Narayanan, C., Lakehal, D., Subramaniam, S., 2006. Accurate numerical estimation of interphase momentum transfer in Lagrangian–Eulerian simulations of dispersed two–phase flows, doi:10.1016/j.ijmultiphaseflow.2007.06.002.

Harris, S. E., Crighton, D. G., 1994. Solitons, solitary waves, and voidage disturbances in gas-fluidized beds. J. Fluid Mech. 266, 243–276.

Kuipers, J. A. M., 1990. A two-fluid micro balance model for fluidized beds. Ph.D. thesis, University of Twente.

O'Rourke, P. J., Snider, D. M., 2010. An improved collision damping time for mp-pic calculations of dense particle flows with applications to polydisperse sedimenting beds and colliding particle jets. Chemical Engineering Science 65 (22), 6014 – 6028.
URL http://www.sciencedirect.com/science/article/pii/S0009250910005075

O'Rourke, P. J., Zhao, P. P., Snider, D., 2009. A model for collisional exchange in gas/liquid/solid fluidized beds. Chemical Engineering Science 64 (8), 1784 – 1797.
URL http://www.sciencedirect.com/science/article/pii/S0009250908006829

Patankar, N., Joseph, D., 2001. Modeling and numerical simulation of particulate flows by the eulerianlagrangian approach. International Journal of Multiphase Flow 27 (10), 1659 – 1684.
URL http://www.sciencedirect.com/science/article/pii/S0301932201000210

Patil, D., van Sint Annaland, M., Kuipers, J., 2005. Critical comparison of hydrodynamic models for gassolid fluidized bedspart i : bubbling gassolid fluidized beds operated with a jet. Chemical Engineering Science 60 (1), 57 – 72.
URL http://www.sciencedirect.com/science/article/pii/S0009250904005007

Snider, D. M., 2001. An incompressible three-dimensional multiphase particle-in-cell model for dense particle flows. Journal of Computational Physics 170 (2), 523 – 549.
URL http://www.sciencedirect.com/science/article/pii/S0021999101967476

Syamlal, M., 1998. Mfix documentation: Numerical guide. Tech. Rep. DOE/MC31346-5824, NTIS/DE98002029, National Energy Technology Laboratory, Department of Energy, see also URL http://www.mfix.org.

Syamlal, M., Rogers, W., O'Brien, T. J., 1993. Mfix documentation: Theory guide. Tech. Rep. DOE/METC-95/1013, NTIS/DE95000031, National Energy Technology Laboratory, Department of Energy, see also URL http://www.mfix.org.

Xu, J., Pope, S. B., 1999. Assessment of numerical accuracy of PDF Monte Carlo methods for turbulent reacting flows. J. Comp. Phys. 152 (1), 192–230.